Hybrid incompatibility emerges at the one-cell stage in interspecies *Caenorhabditis* embryos

Jessica Bloom[1], Rebecca Green[2*], Arshad Desai[2,3], Karen Oegema[2,3], Scott A. Rifkin[1*@]

1 Department of Ecology, Behavior, and Evolution, School of Biological Sciences, University of California, San Diego, La Jolla, CA 92093, USA

2 Department of Cell and Developmental Biology, School of Biological Sciences, University of California, San Diego, La Jolla, CA 92093, USA

3 Department of Cellular and Molecular Medicine, University of California San Diego, La Jolla, California 92093, USA.

[@] Lead Contact: Scott A. Rifkin (sarifkin@ucsd.edu)

[*]Corresponding authors: Scott A. Rifkin (sarifkin@ucsd.edu), Rebecca Green (regreen@ucsd.edu)

SUMMARY:

When genetic differences between populations disrupt the development of hybrid organisms, this prevents gene flow and enforces speciation.[1–3] While prior studies have examined the genetic origins of hybrid incompatibility,[4–17] the effects of incompatible factors on development remain poorly understood. Here, we investigate the mechanistic basis of hybrid incompatibility in *Caenorhabditis* nematodes by capitalizing on the ability of *C. brenneri* females to produce embryos after mating with males from several other species. These hybrids nearly always die, and their developmental problems begin immediately after fertilization, suggesting that post-fertilization barriers to hybridization originate from physical incompatibility between sperm and oocyte-derived factors rather than from zygotic transcription, which starts after the 4-cell stage.[18–21] Sperm deliver chromatin, which expands to form a pronucleus, and a pair of centrioles, which form centrosomes that attach to the sperm-derived pronucleus and signal to establish the embryo's anterior-posterior axis.[22,23] In *C. brenneri* oocytes fertilized with *C. elegans* sperm, sperm-derived pronuclear expansion was delayed, frequent centrosome detachment was observed, and cortical polarity was disrupted. Live imaging revealed that defective polar body extrusion contributes to defects in mitotic spindle morphology. These early problems lead to abnormal embryonic organization in hybrids at the crucial 4-cell stage. *C. brenneri* oocytes fertilized with *C. remanei* or *C. sp. 48* sperm showed similar defects, and their severity and frequency increased with phylogenetic distance. Our results indicate that physical mismatches between sperm and oocyte-derived structures can destabilize development and may be a primary mechanism of hybrid incompatibility.

KEYWORDS: intrinsic reproductive isolation, hybrid incompatibility, Caenorhabditis nematodes, cell polarity

RESULTS AND DISCUSSION

Hybrid embryos of *C. brenneri* females and *C. elegans* males exhibit polarity defects prior to zygotic genome activation

Prior work has shown that *C. brenneri* females can be fertilized by males from different species across the *Elegans* subgroup (confirmed species in dark grey in **Fig. 1A**), although the resulting hybrid embryos inevitably die (**Fig. 1A**).[24–26] To identify the incompatibilities that prevent successful embryonic development, we analyzed *C. brenneri* oocytes fertilized with *C. elegans* sperm, which allows us to take advantage of tools available in *C. elegans*. Brood size, especially on the second day after mating, was consistently smaller in the interspecies cross than for an intraspecies cross of *C. brenneri* (**Fig. 1B**), suggesting that either fewer sperm are transferred in the interspecies cross or that the ability of sperm to remain fertilization competent in the spermatheca is reduced. As anticipated, all of the hybrid embryos died, compared to only 6% (145/2263 embryos) and 2% (56/2991 embryos) respectively, of the intraspecies fertilized *C. brenneri* and *C. elegans* embryos (**Fig. 1B**).

Prior work in other species has shown that mismatches in the timing and regulation of zygotic gene expression can lead to hybrid incompatibility.[12,13,27,28] However, problems could also arise before the onset of zygotic gene expression due to incompatibilities between the interacting components of oocytes and sperm. Based on work in *C. elegans* and other *Caenorhabditis* species, we expect zygotic genome activation to begin at the 4-cell stage (**Fig. 1C**).[18–21] To determine when incompatibility first becomes evident, we mated unmarked *C. brenneri* or *C. elegans* (*fog-2*) females to males from a *C. elegans* strain in which the genome encodes fluorescent reporters that mark nuclei in the endoderm (*green*), mesoderm (*yellow*), and ectoderm (*red*)[29,30] (**Fig. S1A**). We also mated unmarked *C. brenneri* males to *C. brenneri* females for comparison. Since the markers do not turn on until later in development, embryos were initially filmed using differential interference contrast microscopy to monitor events between fertilization and the 4-cell stage (**Fig. 1D-F**). Embryos were then left to develop overnight and imaged the next day to identify the point of arrest and determine whether the tissue-specific markers had turned on (**Fig. S1A-C**).

65 Events between fertilization and the 4-cell stage in *C. elegans* (schematized in **Fig. 1C**) have
66 been extensively studied.[23,31,32] As is typical for metazoans, oocytes lack centrioles/centrosomes[33,34] and
67 the sperm brings a pair of centrioles, along with the paternal chromatin, into the oocyte. The maternal
68 chromatin completes two rounds of meiotic segregation at the anterior end of the embryo to generate two
69 polar bodies and the maternal pronucleus, while the sperm chromatin and centrioles remain quiescent
70 as a compact unit. After the second polar body has been jettisoned, the sperm centrioles recruit a
71 microtubule-nucleating scaffold to form centrosomes, and the pronucleus that has formed around the
72 sperm chromatin begins to expand.[35–37] The nascent centrosomes stay associated with the sperm
73 pronucleus and are sandwiched between the pronucleus and the cortex. The centrosomes send a signal
74 that marks the embryo posterior, which triggers the formation of two antagonistic cortical domains: a
75 posterior domain containing a PAR ("Partitioning-defective") protein complex that includes PAR-2 and an
76 anterior domain containing a PAR protein complex that includes PAR-6 (**Fig. 1D**).[22,23,38–40] The first mitotic
77 spindle divides the embryo between these two domains, generating a larger anterior (AB) cell and smaller
78 posterior (P1) cell. During the second cell division, the spindle in the anterior AB cell sets up vertically
79 (perpendicular to the anterior-posterior axis of the embryo), and the spindle in the posterior P1 cell sets
80 up horizontally (parallel to the anterior-posterior axis of the embryo), which leads to a characteristic
81 organization of the daughters of AB (ABa and ABp) and P1 (P2 and EMS) at the 4-cell stage (ABa on top
82 of EMS in the middle flanked by ABp and P2 on the anterior and posterior sides; **Fig. 1C,D**).[23] Improper
83 organization disrupts cell-cell signaling and cell-fate specification. In *C. elegans*, knocking down *par-2* by
84 RNAi prevents a functional posterior domain from forming, and the spindles in both daughter cells line
85 up vertically (as they would in the anterior AB cell), leading to a 4-leaf clover-like organization at the 4-
86 cell stage (Both Anterior; **Fig.1D, Fig. S1D**).[23,38,39,41,42] Knocking down *par-6* prevents the formation of a
87 functional anterior domain and causes the spindles in both daughter cells to line up horizontally (as they
88 would in the posterior P1 cell), leading to a linear chain of cells at the 4-cell stage (Both Posterior; **Fig.
89 1D, Fig. S1D**).[38,39,41] Similar polarity defects were observed in *C. brenneri* embryos after RNAi of *par-2*
90 and *par-6*, although the *par-6* knockdown led to roughly equivalent numbers of embryos with Both

91 Anterior and Both Posterior phenotypes (**Fig. 1D, Fig. S1D**; **Video S1**). Whereas intraspecies *C. brenneri*
92 and *C. elegans* embryos exhibited a normal 4-cell pattern in 92% (12/13) or 95% (19/20) of cases,
93 respectively, only 7% (3/44) of hybrid embryos resulting from mating *C. elegans* males with *C. brenneri*
94 females did. Instead, 21% (9/44) of hybrid embryos exhibited a Both Anterior phenotype, 9% (4/44)
95 exhibited a Both Posterior phenotype, and 64% (28/44) displayed an aberrant pattern (Other) that
96 typically included an abnormally positioned P1 cell (**Fig. 1E**). To more directly probe polarity
97 establishment in hybrids, we identified a *C. elegans* anti-PAR-2 antibody[43] that also detects the posterior
98 cortical domain in 1-cell stage *C. brenneri* embryos (25/25). Consistent with a polarity defect, all but one
99 hybrid embryo, which properly established a PAR-2 domain, either completely lacked a defined PAR-2
100 domain (3/9) or exhibited an incomplete or misplaced PAR-2 domain (5/9; **Fig. 1F**).
101 To determine whether polarity problems affected the ability of hybrid embryos to reach mid-
102 embryogenesis and turn on tissue-specific markers, we collected DIC and spinning disk confocal
103 fluorescence z-stacks the next day, after the embryos had died (**Fig. S1A-C**). This revealed that the
104 organization of the embryos at the 4-cell stage predicted whether they went on to express the fluorescent
105 germ-layer reporters. Of the three hybrid embryos that exhibited normal morphology at the 4-cell stage,
106 all turned on the germ layer reporters prior to arrest. By contrast, only 11% (1/9) of hybrids exhibiting a
107 Both Anterior polarity phenotype, 25% (1/4) of hybrids exhibiting a Both Posterior polarity phenotype, and
108 38% (10/26) of hybrids exhibiting an Other aberrant 4-cell morphology defect turned on the germ layer
109 reporters prior to arrest (**Fig. S1A-C**). We conclude that hybrid embryos from matings between *C. elegans*
110 males and *C. brenneri* females exhibit problems with cell patterning consistent with a failure to properly
111 establish anterior-posterior polarity and that these polarity defects lead to an inability to properly pattern
112 tissues that express germ layer reporters. Polarity defects are evident prior to zygotic genome activation,
113 suggesting that they arise due to an incompatibility between the components of the oocyte and sperm.
114

115 **Centrioles detach from the sperm pronucleus in hybrid embryos, likely due to delayed sperm**
116 **pronuclear expansion**

117 Next, we wanted to understand the nature of the incompatibility that gives rise to the polarity
118 defects in hybrid embryos. Cortical polarity is established at the one-cell stage when the sperm-provided
119 centrioles recruit a pericentriolar material (PCM) scaffold composed of SPD-5. This recruits γ-tubulin
120 complexes for microtubule nucleation and provides a cue that establishes cortical polarity (**Fig. 2A**).[22,44–
121 46] To determine if sperm-provided *C. elegans* centrioles recruit a PCM scaffold in *C. brenneri* oocytes,
122 we used immunofluorescence to visualize both γ-tubulin, which docks onto the SPD-5 scaffold (**Fig. 2B;**
123 **Fig. S2A,A'**),[45,47] and α-tubulin, to monitor microtubule nucleation (**Fig. S2B**). In both *C. elegans* (12/12)
124 and *C. brenneri* (14/14) embryos, centrosomes adjacent to the sperm pronucleus recruited γ-tubulin, and
125 α-tubulin-containing microtubules emanated from the centrosomes **Fig. 2B; Fig. S2A).** In hybrid embryos,
126 centrosomes also recruited γ-tubulin and nucleated α-tubulin-containing microtubules (**Fig. 2B**; **Fig.**
127 **S2A**;12/12 embryos), indicating that the centrioles from *C. elegans* sperm can form centrosomes that
128 nucleate microtubules in *C. brenneri* oocytes. In *C. elegans* and *C. brenneri*, both centrosomes remain
129 attached to the sperm pronucleus. However, in the hybrids one or both centrosomes frequently detached
130 from the sperm-derived pronucleus (**Fig. 2B**; **Fig. S2A**; 11/12 embryos).

131 The centrosome detachment in the hybrids has the potential to disrupt polarity establishment by
132 preventing the sperm pronucleus from holding the centrosomes in a position adjacent to the cortex where
133 they deposit the polarity cue. Proper centrosome positioning is also important for establishing spindle
134 structure and orientation.[48,49] We investigated centrosome detachment further by tracking centrosome
135 movement in living embryos. We mated unmarked *C. brenneri* or *C. elegans* (*fog-2*) females to males
136 from a *C. elegans* strain expressing an mCherry fusion with the centriolar protein SAS-4 (mCherry
137 centrioles).[47] Unmarked *C. brenneri* males were also mated to *C. brenneri* females as a control. In the *C.*
138 *elegans* embryos, during the interval when polarity establishment occurs,[22,35,38] the two mCherry::SAS-4
139 marked centrosomes separated as the sperm pronucleus came into proximity to the cortex (**Fig. 2C,D**).
140 Throughout this process, both centrosomes remained attached to the sperm pronucleus (Pronuclear
141 Appearance stage; 24/26 embryos; **Fig. 2C,D, Video S2**). Centrosome-pronuclear attachment is

142 mediated by dynein anchored to the pronuclear envelope via the LINC complex,[50–52] which pulls the
143 centrosomes towards the pronuclei by walking towards the minus ends of centrosomally nucleated
144 microtubules. After polarity establishment, the sperm and oocyte pronuclei migrated toward each other
145 (**Video S2**) as the dynein associated with the oocyte pronucleus captured and walked toward the minus
146 ends of the centrosomal microtubules.[50,52] At pronuclear meeting, the centrosomes in the *C. elegans*
147 embryos were positioned above and below the interface between the pronuclei (**Fig. 2E**, Pronuclear
148 Meeting; 25/26 embryos; **Video S2**). Upon pronuclear envelope break-down, the first mitotic spindle
149 formed along the embryo's long axis, with the mCherry containing centrosomes at the two spindle poles
150 (**Fig. S2B, Video S2**). After the cell divided, each daughter cell inherited a centrosome with a single
151 sperm-derived centriole (**Fig. S2B, Video S2;** 26/26 embryos).

152 In contrast, at the pronuclear appearance stage in hybrid embryos, one of the two mCherry-
153 containing centrosomes frequently detached (>9 μm of separation) from the sperm pronucleus and
154 migrated into the cytoplasm or along the cortex (12/15 embryos; **Fig. 2D**). The detached centrosomes
155 were often recaptured prior to or during pronuclear meeting (**Video S2**). Even though centrosomes were
156 recaptured, in 67% of cases (10/15), the centrosomes were improperly positioned relative to the two
157 pronuclei prior to nuclear envelope breakdown (**Fig. 2E**).

158 Similar phenotypes in which one centrosome detaches from the sperm pronucleus and
159 subsequently reattaches prior to pronuclear meeting have been observed following perturbations that
160 reduce the surface area of the sperm pronucleus.[48,53] Experimental data support the idea that the number
161 of centrosomes that can attach to a pronucleus is limited by its surface area. Small pronuclei can only
162 interact with the microtubules from one centrosome, and interaction with microtubules from a second
163 centrosome becomes possible only after pronuclei pass a threshold size.[53] To determine if the size of the
164 sperm pronucleus in hybrids could be the cause of centrosome detachment, we measured the cross-
165 sectional area of the sperm and oocyte pronuclei at pronuclear appearance and pronuclear meeting. At
166 pronuclear appearance, the sperm pronuclei in hybrids were about half the size of those in intraspecies

167 *C. brenneri* and *C. elegans* embryos (**Fig. 2F**). At pronuclear meeting, the hybrid sperm pronuclei
168 remained about half the size of their intraspecies counterparts and of the oocyte pronuclei (**Fig. 2F; Fig.**
169 **S2C**). Even if the second centrosome eventually reattached to either the sperm or oocyte pronucleus,
170 the arrangements of both the centrosomes and pronuclei were abnormal at pronuclei meeting (**Fig. 2E,F**).
171 The *C. elegans* sperm-derived pronucleus is unable to properly expand in the *C. brenneri* oocyte
172 cytoplasm, which likely leads to centrosome detachment from the nucleus and polarity defects.

173

174 **Improperly positioned centrosomes cause defects in spindle orientation, and failures of polar**
175 **body extrusion lead to abnormal spindle morphology**

176 Since centrosomes sit at the poles of the mitotic spindle, aberrant centrosome-pronuclear
177 arrangements at the point of pronuclear meeting could lead to spindle structure defects after nuclear
178 envelope breakdown. Embryonic polarity defects could also contribute to spindle orientation
179 problems.[48,49,54] To analyze spindle orientation, we measured the angle between the centrosome-to-
180 centrosome axis of the spindle and the anterior-posterior axis of the embryo using DIC microscopy (**Fig.**
181 **3B**); in DIC images, centrosomes appear as clear areas devoid of yolk particles. For this analysis, we
182 collected images every 30-45 seconds for 3.5-4.5 minutes starting from the onset of metaphase. Whereas
183 95% (161/168) of spindle orientations were between -7.5° and 10.6° of the anterior-posterior axis in
184 control embryos, only 37% were in this range for hybrid embryos, which instead exhibited spindle angles
185 between -56° and 51°. The spindle orientation problems in hybrid embryos are consistent with the defects
186 in cortical polarity, which is associated with large oscillations off the longitudinal axis at anaphase (**Fig.**
187 **1B**).[54]

188 To visualize spindle structure, we mated unmarked *C. brenneri* or *C. elegans* (*fog-2*) females to
189 males from a *C. elegans* strain expressing the mCherry-tagged centriolar protein SAS-4 as before and
190 dissected the worms into media containing SiR-Tubulin, a vital dye that stains microtubules. *C. elegans*
191 and *C. brenneri* embryos had centrosomal microtubule asters at the two spindle poles and robust arrays

192 of kinetochore microtubules pointed toward the centrally-aligned chromosomes (**Fig. 3C,D, Video S3**).
193 In hybrids, 19/22 hybrid embryos exhibited abnormal spindle morphologies. These included arrays of
194 kinetochore microtubules (spindle arms) that pointed in random directions instead of towards the other
195 centrosome, most likely because the centrosome was attempting to capture chromosomes that were in
196 an atypical position when nuclear envelope breakdown occurred (**Fig. 3C,D**; **Fig. S2C; Video S3**). In
197 8/22 of hybrid embryos, the mitotic spindle microtubules appeared to capture remnants of the meiotic
198 spindle in the anterior of the embryo that had segregated the oocyte-derived chromosomes into the polar
199 body (**Fig. 3C,D**). In these cases, the mitotic spindle appeared to pull a part of the meiotic spindle into
200 the cytoplasm and/or to engage meiotic chromosomes. The continued presence of the meiotic spindle in
201 the mitotic cytoplasm, suggests that embryo failed to successfully jettison of one set of sister chromatids
202 into the 2nd polar body at the end of meiosis II.[55] We also analyzed spindles by immunofluorescence,
203 staining for γ-tubulin and microtubules and confirmed the presence of spindles with anomalous
204 morphology (7/15 embryos). We frequently observed chromosomes surrounding the centrosomal asters
205 (10/15 embryos; **Fig 3E**) in hybrids and never in *C. elegans* or *C. brenneri* embryos. These chromosomes
206 had a morphology consistent with meiotic chromosomes, supporting the conclusion that extrusion of the
207 2nd polar body frequently fails in hybrid embryos and leads to defects in spindle morphology.
208

209 **A similar suite of early defects is observed in hybrids of crosses between *C. brenneri* females and**
210 **males from three Elegans group species**

211 We have shown that the inviability of hybrids from female *C. brenneri* and male *C. elegans* starts
212 with problematic interactions between the components of the oocyte and sperm after fertilization, well
213 before any mis-regulation of zygotic gene expression. In addition to *C. elegans*, C*. brenneri* females are
214 able to be fertilized by males of many other species in the *Caenorhabditis Elegans* subgroup.[24,25] Nearly
215 all of these hybrid offspring die during embryogenesis, which is common for hybrids between various
216 *Caenorhabditis* species.[24,25] To determine whether the fatal incompatibilities are different for each species
217 pair and whether the severity of the developmental defects increase with phylogenetic distance, we

218 analyzed hybrid embryos from two additional crosses to *C. brenneri* females: *C. sp. 48* and *C. remanei*.
219 *C. brenneri* and *C. elegans* are separated by around 200 million generations (or around 35 million years
220 of evolution), although these estimates have wide uncertainty (Cutter 2008). *C. sp. 48* is a sister species
221 of *C. brenneri*, about a third as divergent at the amino acid level from *C. brenneri* as *C. elegans*. *C.*
222 *remanei* has a more recent common ancestor with *C. brenneri* than *C. elegans*, but its protein sequences
223 are on average around 17% more divergent (**Fig. 4A**). Compared to intraspecies crosses, *C. brenneri*
224 females had a reduced brood size after mating with *C. remanei*, and, although nearly all embryos died,
225 a few were able to hatch (2/887) (**Fig. 4B**). *C. brenneri* females crossed to *C. sp. 48* males had brood
226 sizes comparable to intraspecies crosses, but the resulting embryos all died during embryogenesis (**Fig.**
227 **4B**).

228 To document the range of early embryonic defects, we scored DIC movies of ~120 embryos from
229 *C. brenneri, C. sp. 48, C. remanei*, and *C. elegans* as well as hybrids between *C. brenneri* females and
230 the three other species for the presence of 20 distinct early embryonic defects (**Fig. 4C,D; Fig. S3A,**
231 **Table S1**). All of the hybrids exhibited a similar spectrum of early defects, including small and/or
232 misshapen sperm pronuclei, centrosome detachment, and a "cross-eyed" phenotype indicative of
233 chromosome mis-segregation.[48] We also observed evenly sized AB and P1 cells at the 2-cell stage and
234 abnormal cell patterns at the 4-cell stage indicative of cell polarity defects (**Video S4)**. Defects in the
235 more distant *C. remanei* and *C. elegans* crosses were more frequent and severe compared to the sister
236 species cross and included failures of both polar body extrusion and cytokinesis.

237

238 **Conclusion**

239 Incompatibility between interacting components in the oocytes and sperm may be a common
240 mechanism underlying hybrid incompatibility between nematodes of the *Caenorhabditis Elegans*
241 subgroup (**Fig. 4E)**. A major driver of sperm incompatibility with *C. brenneri* oocytes is a delay in
242 expanding the sperm-derived pronucleus. Prior work suggests that a small sperm pronucleus would lead
243 to centrosome detachment,[48,53] which we frequently observed in hybrid embryos. Centrosome

244 detachment, in turn, could cause the observed defects in cell polarity (**Fig. 4F**). It is also possible that the
245 microtubule asters of detached centrosomes may aberrantly capture the meiosis II spindle, leading to the
246 polar body extrusion defects we observed. It will be interesting to see if delayed expansion of the sperm-
247 derived pronucleus is a feature specific to hybrids with *C. brenneri* females, which might be a valuable
248 adaptation for a species that tolerates promiscuous fertilization, or whether it is a more general feature
249 of hybrids between different species pairs across the *Elegans* group.

250 The fact that *C. brenneri*/*C. sp. 48* hybrids often overcome their initial problems to reach a
251 superficially normal 4-cell stage (**Fig. 4D**), suggests that while there are incompatibilities that destabilize
252 early development, the severity of destabilization increases with greater evolutionary distance between
253 the parents. The variability in development between hybrid embryos, even within a cross, is consistent
254 with the idea that many developmental events are less robust in hybrids than in intraspecies embryos
255 and fail at appreciable frequency. Although a few hybrid embryos may thread the needle to find a narrow
256 pathway to hatching, most fall victim to a series of stochastic failures that build on each other to a fatal
257 outcome (**Fig. 4F**). These failures that cause hybrid incompatibility begin in the zygote almost
258 immediately after fertilization and well before the activation of developmental gene expression programs.

ACKNOWLEDGEMENTS

We would like to thank members of the Rifkin, Oegema, and Desai labs for helpful discussions. We would like to thank the Hyman lab for the generous gift of the PAR-2 antibody. We would like to Marie-Ann Felix for the generous gift of strain BRC20359 (*C. sp. 48*). We would also like to thank Anthony Ye and Aidan Linkins for their help. This work was supported by grants from the NIH (GM103782) and the NSF IOS (1936674) to S.A.R. and from the NIH to K.O. (GM147265). A.D. and K.O. received salary and other support from the Ludwig Institute for Cancer Research. JB was partially supported by NIH/NIGMS (T32 GM127235). Some strains were provided by the CGC, which is funded by NIH Office of Research Infrastructure Programs (P40 OD010440).

AUTHOR CONTRIBUTIONS

Conceptualization: J.B., R.G., K.O., S.A.R.; Methodology: J.B., R.G., K.O., S.A.R.; Formal analysis: J.B., R.G.; Investigation: J.B., R.G.; Resources: S.A.R., K.O.; Data curation: J.B., R.G.; Writing - original draft: J.B., R.G., K.O., S.A.R.; Writing - review & editing: J.B., R.G., A.D., K.O., S.A.R.; Visualization: J.B., R.G.; Supervision: S.A.R., K.O.; Project administration: S.A.R., K.O.; Funding acquisition: S.A.R., K.O.

DECLARATION OF INTERESTS

The authors declare no competing interests.

MAIN FIGURES WITH TITLES AND LEGENDS

Bloom et al., Figure 1

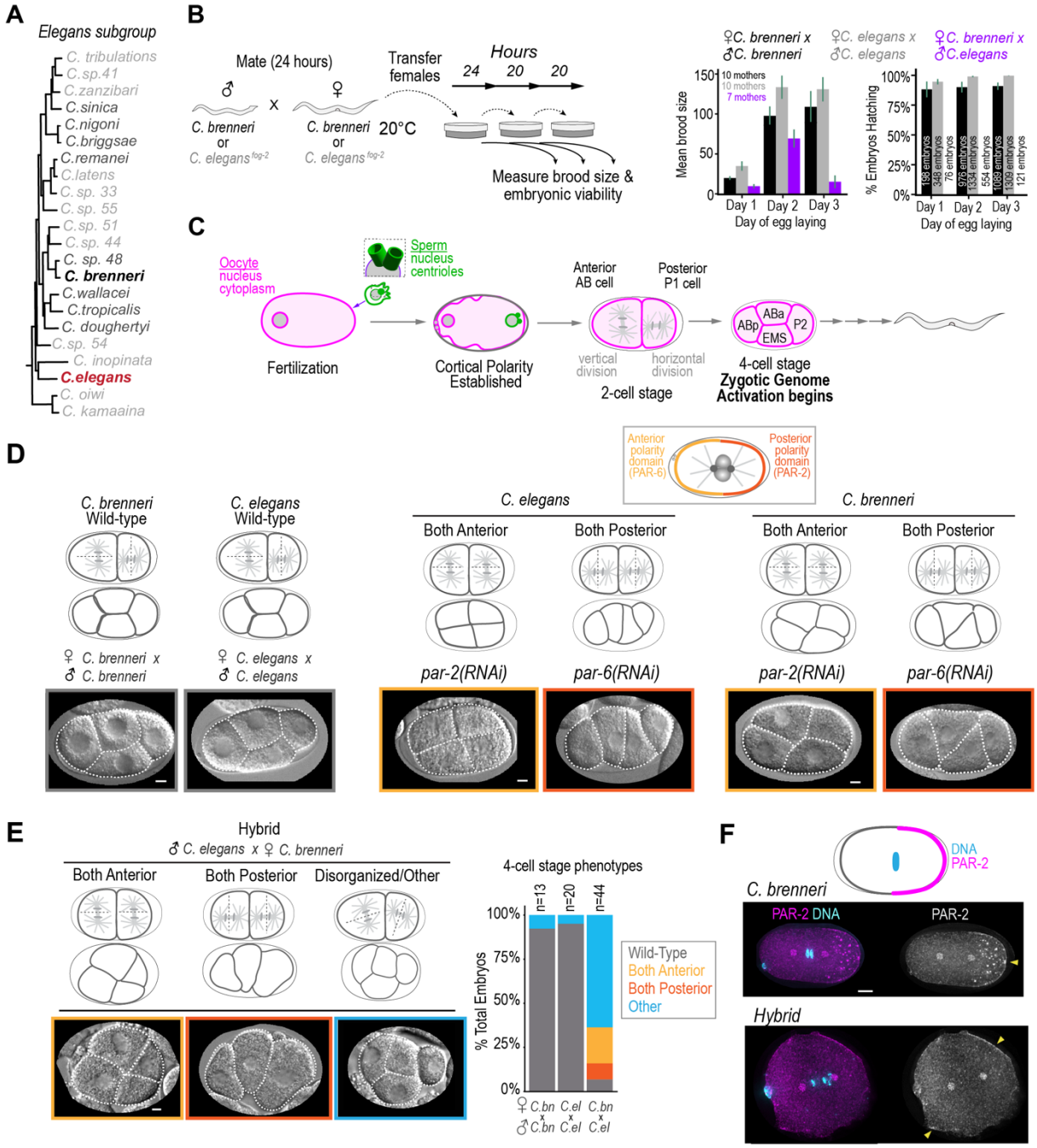

279

280 **Figure 1**. **Hybrid embryos resulting from fertilization of *C. brenneri* oocytes with *C. elegans* sperm exhibit**
281 **polarity defects prior to zygotic genome activation.** (**A**) Phylogeny of the *Caenorhabditis* Elegans subgroup. *C.*
282 *brenneri* females have been shown to be cross-fertile with *C. elegans* (*red*) males and males from the species
283 marked in dark grey. (**B**) Schematic illustrating how embryos were collected after mating. Graphs show the average
284 brood size and % hatching for the embryos collected during each day of egg laying. Day 1 is 0-24 hours post-mating;
285 day 2 is 24-44 hours post-mating; day 3 is 44-64 hours post-mating. Error bars are ± SE. **(C)** Schematic of the
286 events between fertilization and the 4-cell stage when Zygotic Genome Activation (ZGA) begins. The sperm brings
287 in a pair of centrioles along with the sperm chromatin into the oocyte. Hybrid incompatibility could arise due to
288 misregulation of gene expression after ZGA or before ZGA, due to incompatibilities between the structural
289 components of sperm and oocyte. (**D**) Differential interference contrast (DIC) images of 4-cell stage embryos are
290 shown for: (*left*) control intraspecies *C. brenneri* and *C. elegans* embryos; (*middle*) *par-2(RNAi)* and *par-6(RNAi) C.*
291 *elegans* embryos; and (*right*) and *par-2(RNAi)* and *par-6(RNAi) C. brenneri* embryos. For phenotypic quantification
292 see *Fig. S1D*. The schematic on top illustrates the anterior PAR-6 (*yellow*) and posterior PAR-2 (*orange*) domains
293 at the 1-cell stage in *C. elegans*. Schematics immediately above the images show the expected cell and spindle
294 orientations for two-cell and four-cell stage embryos for each condition. (**E**) DIC images illustrating the three non-
295 wild-type classes of 4-cell stage phenotypes observed for hybrid embryos resulting from mating *C. brenneri* females
296 with *C. elegans* males (Both Anterior, Both Posterior, and Disorganized/Other). Schematics above the images
297 illustrate the cell and spindle orientations at the two-cell and four-cell stages for each embryo. The graph quantifies
298 the percentage of embryos that appeared wild-type or exhibited each phenotype. (**F**) (*top*) Schematic illustrating the
299 localization of PAR-2 and DNA in a control embryo. **(***left***)** Representative immunofluorescence images of *C. brenneri*
300 (top; n = 25) and hybrid embryos (bottom; n = 9) stained for PAR-2 (*magenta*) and DNA (*cyan*). (*right*) Grayscale
301 PAR-2 images with yellow arrowheads marking the PAR-2 domains. Scale bars represent 5μm.

Bloom et al., Figure 2

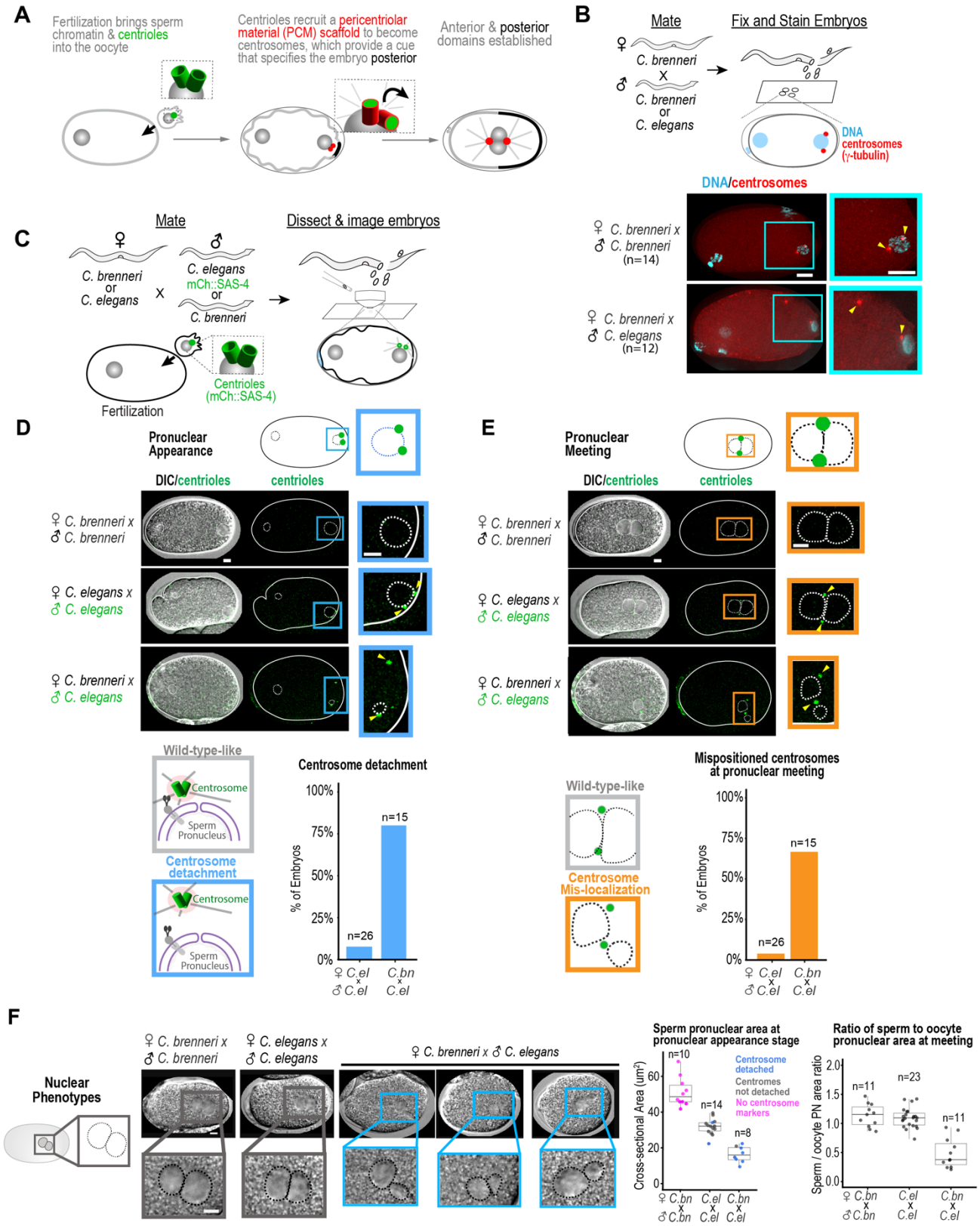

302

303 **Figure 2.** ***Centrioles detach from the sperm pronucleus in hybrid embryos, likely due to delayed sperm***
304 ***pronuclear expansion.*** (**A**) The schematic illustrates how fertilization triggers polarity establishment in the 1-cell
305 embryo. The sperm brings in a pair of centrioles (*green*) that are converted to centrosomes (*red*) via the recruitment
306 of the PCM scaffold protein SPD-5 from the oocyte cytoplasm. The centrosomes, which are sandwiched between
307 the sperm pronucleus and the cortex, provide a cue that specifies the embryo posterior. (**B**) (*top*) The schematic
308 illustrates the mating regime and markers shown in the immunofluorescence images below. (*bottom*)
309 Representative images of 1-cell stage *C. brenneri* (n = 14) and hybrid (n = 12) embryos after the conversion of
310 centrioles to centrosomes, but prior to pronuclear migration, stained for DNA (cyan) and γ-tubulin (red). Insets are
311 magnified 1.7X. γ-tubulin (red) is scaled equivalently in the two images. (**C**) The schematic illustrates the mating of
312 *C. brenneri* or *C. elegans* females with *C. elegans* males whose centrioles are stably marked with mCherry::SAS-4
313 (*green*) to allow monitoring of sperm centriole position throughout the first cell division. (**D**) (*Top*) Paired
314 DIC/fluorescence overlay (*left*) and fluorescence-only (*right*) images of *C. brenneri*, *C. elegans,* and hybrid
315 pronuclear appearance stage 1-cell embryos. The schematic on top illustrates the expected position of the
316 mCherry::SAS-4 marked centrioles adjacent to the sperm pronucleus (*green*). The white solid lines trace the embryo.
317 The white dashed lines trace pronuclei in DIC and fluorescence images. Insets are magnified 2.5X, and yellow
318 arrowheads mark centrosomes. (*Bottom*, *left*) The schematics depict wild-type-like attachment (*grey box*) and
319 aberrant detachment (*blue box*) of centrosomes from the sperm pronucleus. (*Bottom*, *right*) The graph quantifies
320 the percentage of embryos with centriole detachment (>9 μm separation) from the sperm pronucleus. (**E**) (*Top*)
321 Paired DIC/fluorescence overlay (*left*) and fluorescence-only (*right*) images of *C. brenneri*, *C. elegans,* and hybrid
322 pronuclear meeting stage 1-cell embryos. The schematic on top illustrates the expected position of the
323 mCherry::SAS-4 marked centrioles (*green*) above and below the interface between the maternal and paternal
324 pronuclei. The white solid lines trace the embryo. The white dashed lines trace pronuclei in DIC and fluorescence
325 images. Insets are magnified 2.3X, and yellow arrowheads mark centrosomes. (*Bottom*, *left*) The schematics depict
326 wild-type-like positioning of the centrosomes above and below the interface between the maternal and paternal
327 pronuclei (*grey box*) and mispositioning of the centrosomes and nuclei (*orange box*). (*Bottom*, *right*) The graph
328 quantifies the percentage of embryos with mispositioned centrosomes at pronuclear meeting. (**F**) DIC images of
329 representative *C. brenneri*, *C. elegans*, and *hybrid* embryos at pronuclear meeting. Insets are magnified 2X (the
330 black dotted lines trace pronuclei). The left graph plots the cross-sectional area of sperm pronuclei at the pronuclear
331 appearance stage. Median (IQR) for sperm pronuclear cross-sectional area is 49 (39-58), 32 (28-37), and 16 (9-23)
332 μm^2 for *C. brenneri*, *C. elegans*, and hybrid embryos, respectively. Centriole detachment is indicated by blue circles,
333 and wild-type-like centriole separation is indicated by gray circles. In *C. brenneri*, centrioles were not labeled and
334 detachment was not scored (*pink circles*). The right graph plots the ratio of sperm to oocyte pronuclear area at
335 pronuclear meeting (also see *Fig. S2C*). Median (IQR) for sperm pronuclear area to oocyte pronuclear area is 1.2
336 (0.9-1.5), 1.1 (0.9-1,3), 0.4 (0.01-0.73) for *C. brenneri*, *C. elegans*, and hybrid embryos, respectively. Scale bars
337 represent 5μm.

Bloom et al., Figure 3

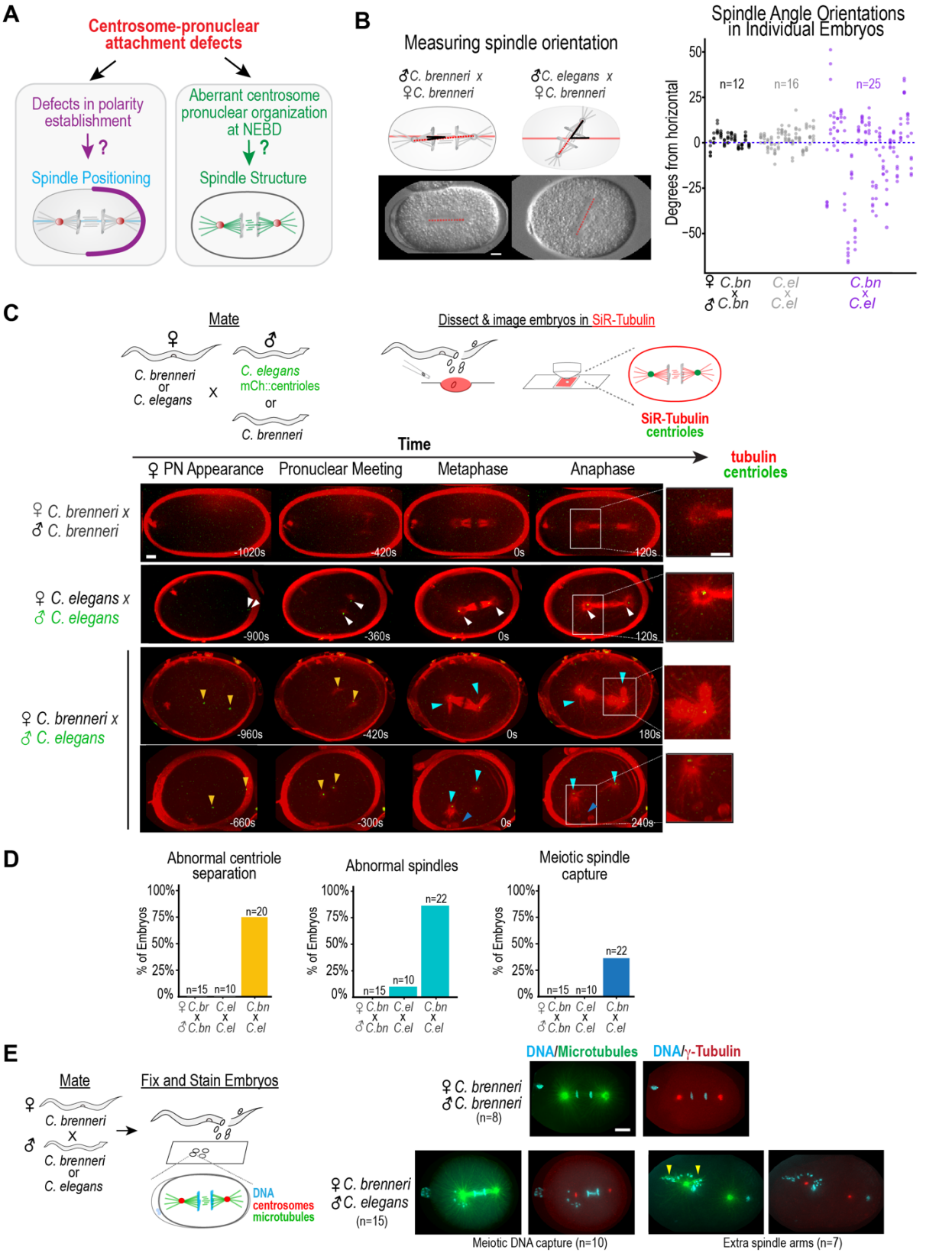

338

339 **Figure 3. *Caenorhabditis* hybrid embryos exhibit defects in spindle orientation, polar body extrusion, and**
340 **spindle morphology** (**A**) A schematic illustrating how detachment of centrosomes from the sperm pronucleus could
341 contribute to defects in polarity establishment, spindle positioning, and spindle morphology in the early embryo. (**B**)
342 Schematics (*top*) and images (*bottom*) illustrating how spindle orientation was assessed. At each timepoint, the
343 angle between the centrosome-to-centrosome axis of the spindle (red dashed line) and the anterior-posterior axis
344 of the embryo (red solid line) was measured. For each embryo six measurements were made at 30-45s intervals
345 starting at metaphase. The graph plots the six measured angles for each embryo in a vertical row. Angles were
346 measured in *C. brenneri* (*black*), *C. elegans* (gray) or hybrid (*purple*) embryos. (**C**) (*Top*) A schematic illustrating
347 how *C. brenneri* or *C. elegans* females were mated with *C. elegans* males with mCherry::SAS-4-marked centrioles
348 to enable live tracking of centrioles (*green*). *C. brenneri* females were also mated with *C. brenneri* males as a control.
349 Embryos were dissected into the vital dye SiR-Tubulin (*red*) to monitor microtubules. Images are maximum intensity
350 projections of representative intraspecies *C. brenneri* and *C. elegans* embryos and hybrids. Times are seconds
351 relative to metaphase. White and yellow arrows indicate proper or improper centriole separation, respectively. Cyan
352 arrows indicate abnormal spindle morphology. Dark blue arrows indicate meiotic DNA capture. Insets (right) show
353 2X magnifications of one anaphase spindle pole as indicated. Maximum intensity projections were made of all z-
354 planes containing the centrosomes and spindle structures, and SiR-Tubulin intensities were scaled to best show
355 spindle morphology and cannot be directly compared. (**D**) The graphs quantify the percentage of embryos exhibiting
356 abnormal centriole separation (*yellow*), abnormal spindle morphology (*cyan*), and meiotic DNA capture (*blue*) for
357 the indicated conditions. (**E**) (*Left*) The schematic illustrates the mating regime and markers shown in the
358 immunofluorescence images to the right. (*Right*) Representative immunofluorescence images of *C. brenneri* (n = 8)
359 and hybrid (n = 15) embryos stained for DNA (*cyan*), microtubules (DM1-α) (*green*) and γ-tubulin (*red*). Two hybrid
360 examples are shown to illustrate the range of hybrid phenotypes, including meiotic DNA capture and extra spindle
361 arms (yellow arrowheads). The scale bar represents 5μm.

Bloom et al., Figure 4

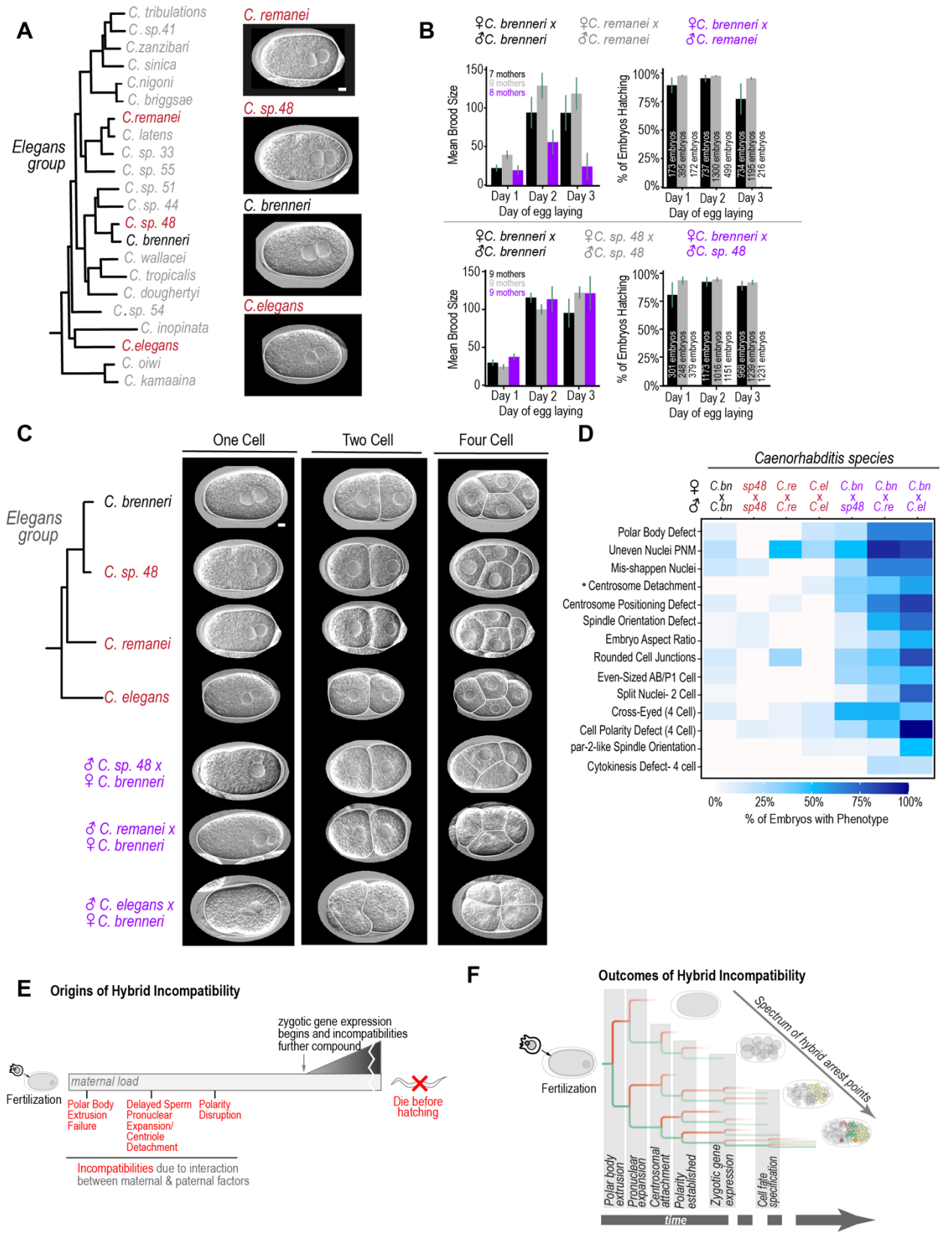

362

363 **Figure 4**. **A similar suite of early defects is observed in hybrid embryos generated by fertilization of *C.***
364 ***brenneri* oocytes with sperm from three Elegans group species. *(*A**) (*Left*) Phylogeny of the *Elegans* subgroup.
365 In subsequent experiments, *C brenneri* (*black*) females were mated with males from three species *C. remanei, C.*
366 *sp. 48,* and *C. elegans (indicated in red).* (*Right*) DIC images of embryos from intraspecies crosses from each of
367 the indicated species; embryos are shown at pronuclear meeting. (**B**) Graphs show the average brood size and %
368 hatching for the embryos collected during the indicated days for the indicated species (*grey*, *black*) or hybrid (*purple*)
369 cross. Day 1 is 0-24 hours post-mating; day 2 is 24-44 hours post-mating; day 3 is 44-64 hours post-mating. Error
370 bars are ± SE. (**C**) DIC images from timelapse series of representative embryos showing them at the 1, 2, and 4-
371 cell stages for all intraspecies (*red and black labels*) and interspecies crosses (*purple labels*). Solid white lines trace
372 the outline of each cell, dotted white lines trace all pronuclei and nuclei. (**D**) The heatmap summarizes embryonic
373 defects observed through the 4-cell stage for the indicated crosses; embryos were scored blinded to cross. The
374 shading goes from no (*white*) to all (*dark blue*) of the embryos displaying the specified phenotype. (*) Identification
375 of centrosome positioning may be hindered compared to centrosome tracking in *Figure 2D* and *E* because
376 centrosomes were tracked using only DIC images. (**E**) A schematic summarizing the early effects of hybrid
377 incompatibility, prior to zygotic genome activation and highlighting several key events that occur less reliably in
378 hybrid embryos. (**F**) Schematic summarizing how the range of phenotypes observed in hybrid embryos results from
379 the fact that a number of early embryonic events become more prone to failure. Embryos in which multiple events
380 fail sequentially exhibit more severe phenotypes and die sooner. Scale bars represent 5μm.

381

382 **SUPPLEMENTAL FIGURE TITLES AND LEGENDS**

Bloom et al., Figure S1

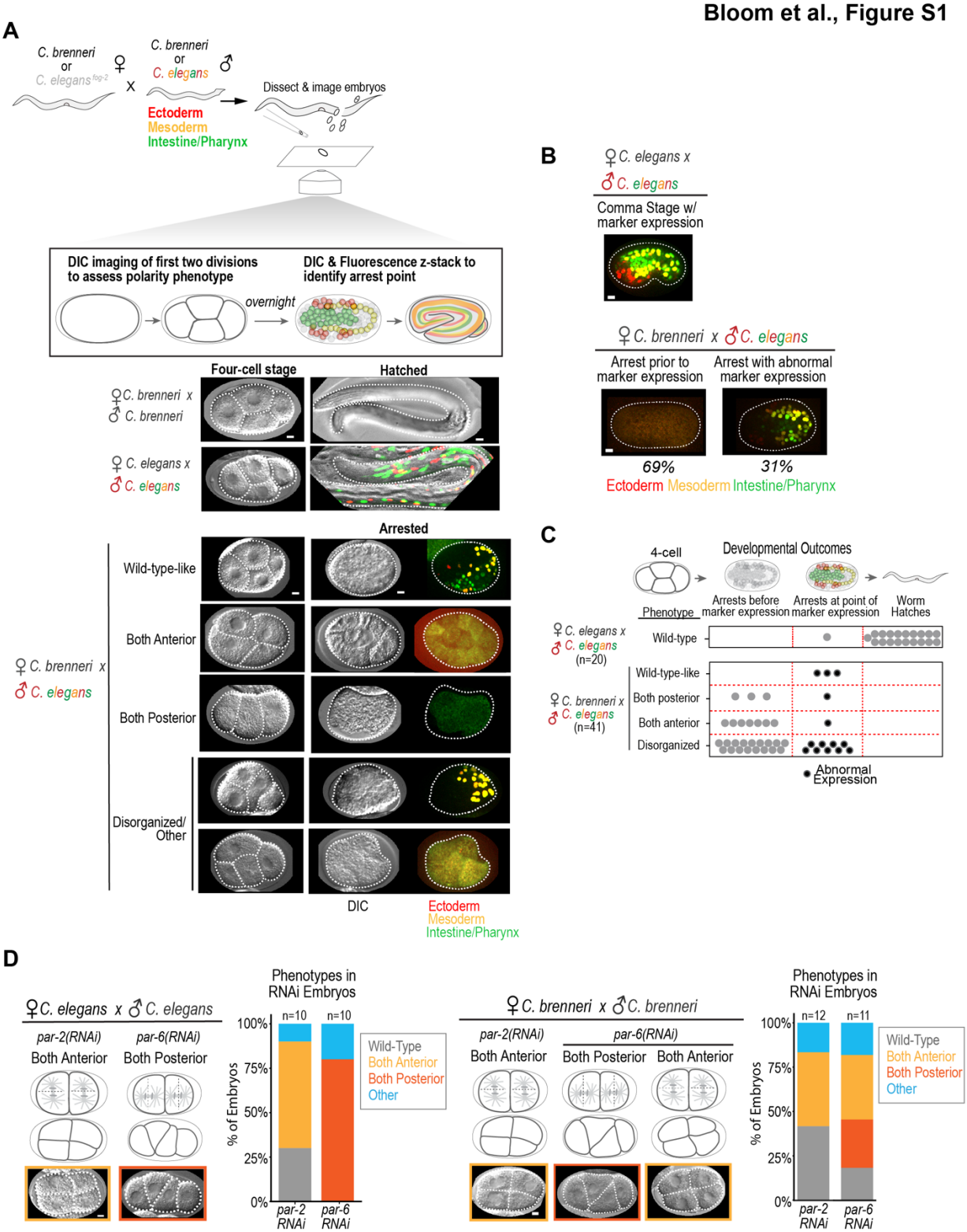

383

384 **Figure S1. Polarity phenotypes at the 4-cell stage correlate with the ability of hybrid embryos to reach mid-**
385 **embryogenesis and turn on tissue-specific markers. (A)** The schematic illustrates the experimental workflow to
386 detect early defects before ZGA, which occurs at the 4-cell stage, and correlate them with the ability of embryos to
387 reach mid-embryogenesis and turn on tissue-specific markers. Briefly, *C. brenneri* or *C. elegans* (*fog-2)* females
388 were mated to males from either *a C. elegans* strain in which the genome encodes fluorescent reporters that mark
389 nuclei in the endoderm (*green*), mesoderm (*yellow*), and ectoderm (*red*) or *C. brenneri*. DIC imaging was used to
390 film embryos through the 4-cell stage. A spinning disk confocal fluorescence z-stack was collected of the same
391 embryos 20-24 hours later to identify the point of arrest and determine whether the tissue-specific markers had
392 turned on. Endpoint images for larval worms are scaled to best highlight marker expression, and intensity levels are
393 not directly comparable to the arrested hybrid embryos. **(B)** Representative maximum intensity projections of
394 spinning disc confocal z-stacks of hybrid embryos that arrested prior to (*bottom left*) and after (*bottom right*) the
395 onset of marker expression compared to the comma stage in control *C. elegans* intraspecies embryos (*top*). Image
396 projections are scaled to best highlight marker expression and intensities cannot be directly compared between *C.*
397 *elegans* and hybrid embryos. (**C**) Summary table displaying the results of the phenotypic analysis for the *C. elegans*
398 and *C. brenneri* x *C. elegans* hybrid embryos. While the majority of *C.* elegans embryos (19/20) showed a wild-type
399 4-cell phenotype and hatched, most hybrid embryos (38/41) showed a non-wild-type-like 4-cell phenotype, and
400 none hatched. All 3 of the hybrid embryos that exhibited a wild-type-like 4-cell orientation survived to express
401 markers, whereas embryos exhibiting more severe polarity phenotypes rarely made it to marker expression (Both
402 Anterior (1/4); Both Posterior (1/9)). Hybrid embryos that fell into the Disorganized/Other category had an
403 intermediate level of success with 9/26 surviving to the point of marker expression. **(D)** DIC images of representative
404 4-cell stage embryos are shown for *par-2(RNAi)* and *par-6(RNAi) C. elegans* (*left*) and *C. brenneri* (*right*) embryos.
405 The schematics highlight the 2-cell division planes giving rise to the 4-cell phenotypes, and the graphs show the
406 phenotype frequencies for each condition. Scale bars represent 5μm.

Bloom et al., Figure S2

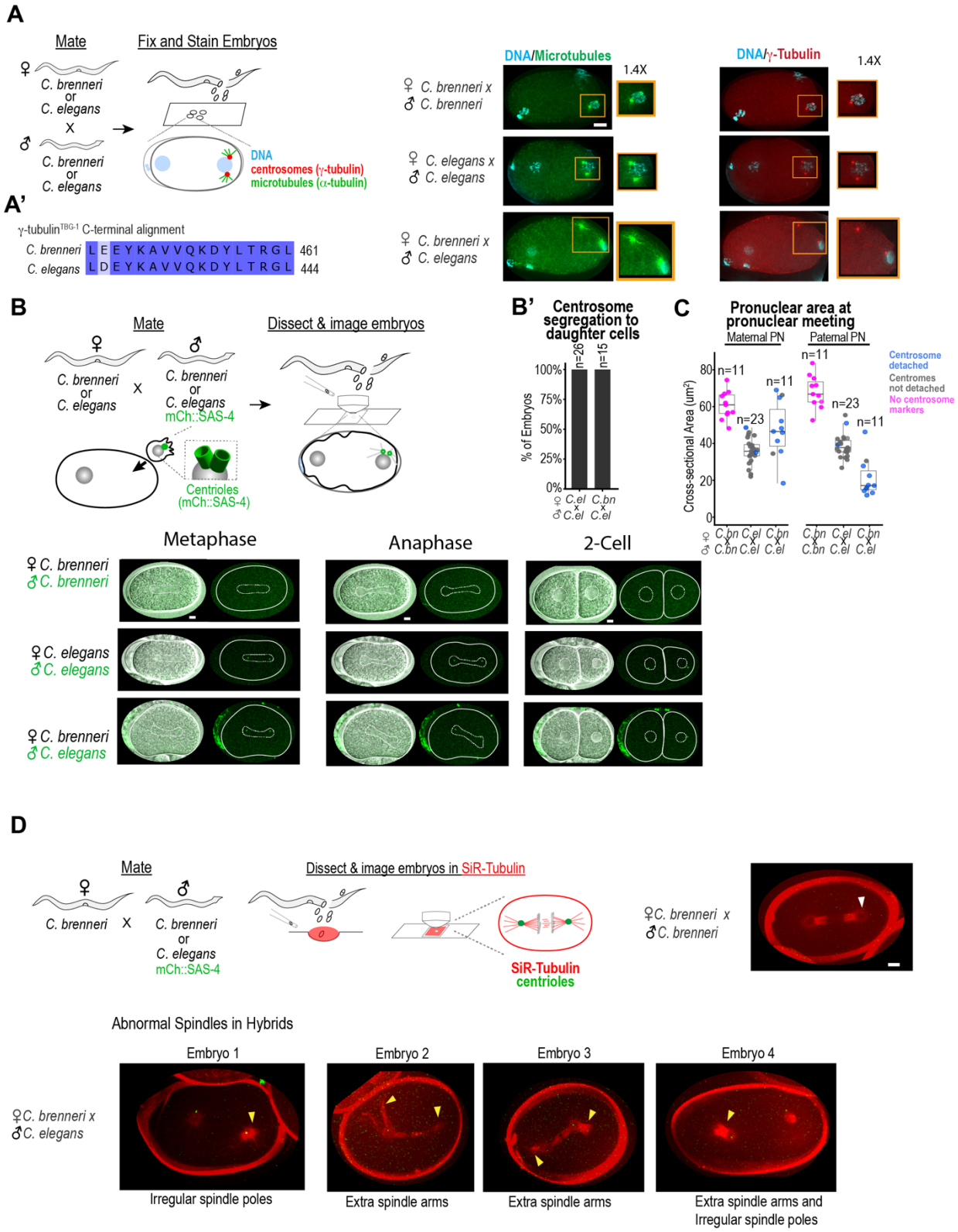

407

408 **Figure S2. Hybrids exhibit abnormal centrosome-pronuclear attachment, polar body extrusion, male**
409 **pronuclear expansion and spindle morphology (A)** (*Left*) The schematic illustrates the mating regime and the
410 predicted staining pattern of α-tubulin, γ-tubulin and DNA after the conversion of centrioles to centrosomes but prior
411 to pronuclear migration. (*Right*) Representative images of 1-cell stage *C. brenneri* (n = 14), *C. elegans* (n=12), and
412 hybrid (n = 12) embryos after the conversion of centrioles to centrosomes but prior to pronuclear migration, stained
413 for DNA (*cyan*), α-tubulin (DM1-α) (*green*), and γ-tubulin (*red*). Insets are magnified 1.4X. One or both centrosomes
414 were often detached in hybrids (11/12 embryos). Maximum intensity projections were scaled to best highlight protein
415 localization, so intensity levels are not directly comparable across images. **(A')** Amino acid alignment of the C-
416 terminal peptide of *C. elegans* γ-tubulin (TBG-1) against which the antibody was raised to the equivalent region of
417 the *C. brenneri* protein. All but one residue is conserved. **(B)** (*Top*) A schematic of mating combinations of *C.*
418 *brenneri* or *C. elegans* females and *C. brenneri* males or *C. elegans* males with mCherry::SAS-4 (*green*) to enable
419 centriole tracking. (*Bottom*) Paired DIC/fluorescence overlay (*left*) and fluorescence-only (*right*) images of *C.*
420 *brenneri*, *C. elegans,* and hybrid embryos at metaphase and anaphase of the first division and at the 2-cell stage.
421 White solid lines (embryo outline) and white dotted lines (pronuclei/nuclei/spindle) are the same across DIC and
422 fluorescence images. Images are different timepoints taken from the timelapse series of the same embryos shown
423 in *Figure 2D & E*. **(B')** Centriole segregation is not affected in hybrid embryos. The graph plots the percent of
424 embryos with marked centrioles that show segregation of one sperm-derived centriole into each daughter cell (26/26
425 embryos in *C. elegans*; 15/15 embryos in hybrids). (**C**) The graph plots the cross-sectional area of the oocyte and
426 sperm pronuclei at pronuclear meeting for the indicated crosses. Centriole detachment is indicated by blue circles
427 and wild-type-like centriole separation by the gray circles. In *C. brenneri*, centrioles were not labeled and
428 detachment was not scored (*pink circles*). Median (IQR) for female pronuclear cross-sectional area is 61 (51-71),
429 36 (30-42), 46 (26-66) μm^2 for *C. brenneri, C. elegans*, and hybrid embryos, respectively. Median (IQR) for male
430 pronuclear cross-sectional area is 67 (56-78), 38 (32-44), 17 (7-27) μm^2 for *C. brenneri, C. elegans*, and hybrid
431 embryos, respectively. (**D**) The schematic (*top, left*) illustrates how *C. brenneri* females were mated with *C. brenneri*
432 males as a control or with *C. elegans* males with mCherry::SAS-4-marked centrioles to enable live tracking of
433 centrioles (*green*), and how embryos were dissected into the vital dye SiR-Tubulin (*red*) to monitor microtubules.
434 Images show maximum intensity projections that capture SiR-Tubulin-stained spindles in a *C. brenneri* embryo (*top,*
435 *right)* and four examples of hybrid embryos (*bottom*) at anaphase. The white arrowhead indicates normal spindle
436 morphology, whereas yellow arrowheads point to spindle poles or extra spindle arms in hybrid embryos. Embryos
437 categorized as having abnormal spindles in the graph in *Figure 3D* displayed phenotypes similar to the ones shown
438 here. Intensities were scaled to best show SiR-Tubulin signal and cannot be compared across embryos. Maximum
439 intensity projections were made to include slices containing centrioles. Centriole intensities are scaled the same
440 across images. *C. brenneri* embryos do not contain marked centrioles. Scale bars represent 5μm.

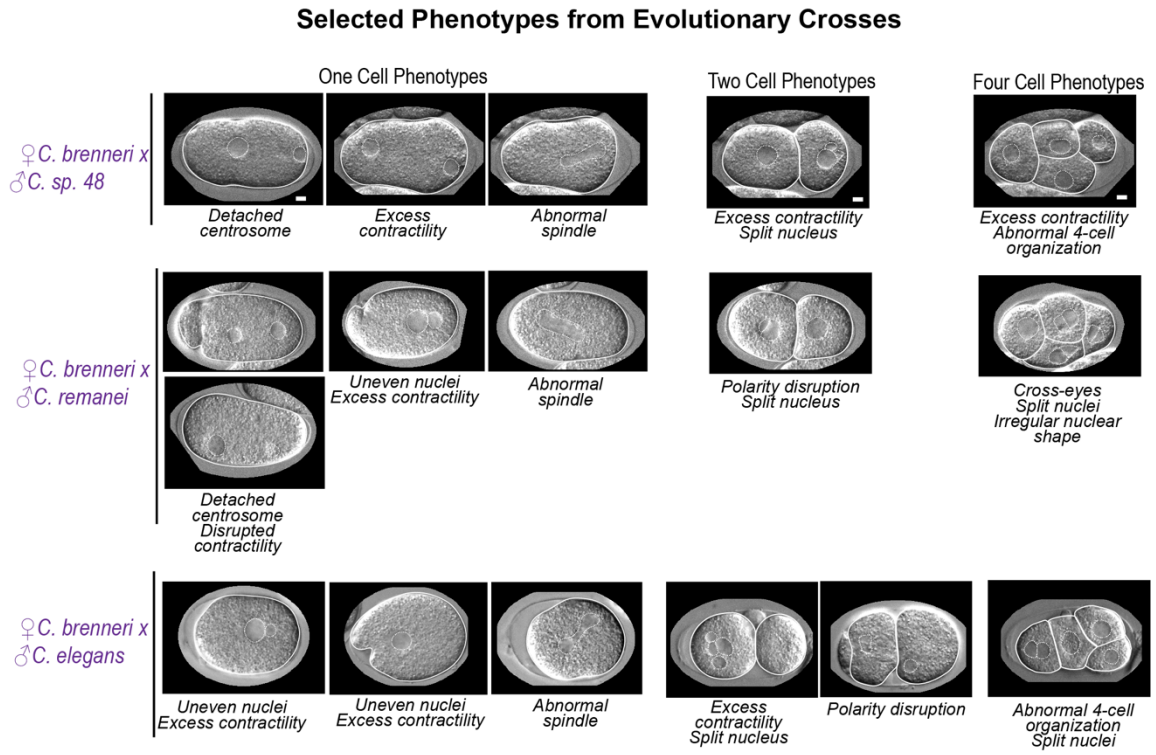

Figure S3. Gallery of hybrid phenotypes. Gallery of 1, 2, 4-cell hybrid embryos from *C. brenneri* females crossed with males from *C. sp. 48* (*top*), *C. remanei* (*middle*), and *C. elegans* (*fog-2(q71)*) (*bottom*). Embryos were dissected and monitored by DIC through the first two cell divisions. Embryos were blind-scored for phenotypes in time-lapse images. The gallery highlights abnormal phenotypes found in 1 to 4-cell embryos. White solid lines outline the embryo and white dotted lines outline the pronuclei, spindle, and nuclei. The scale bar represents 5μm.

Video S1. Similar phenotypes are observed after RNAi of *par-2* and *par-6* in *C. elegans* and *C. brenneri* (related to Figure 1D-F). Timelapse sequences of C. brenneri (*top row*) and *C. elegans* embryos (*bottom row*). Control embryos are shown on the left, *par-2(RNAi)* embryos in the middle and *par-6(RNAi)* embryos on the right. Still images of the *C. brenneri par-6(RNAi)* and *par-2(RNAi)* embryos shown here are also shown in *Figure 1E*. Cleavage sites in the *par-2(RNAi)* (*yellow arrows*) and *par-6(RNAi)* (*orange arrows*) embryos are indicated. 26 x 1um z-stacks were collected every 30 seconds and movies were created by compiling the best z-slice from the z-stack collected at each timepoint. Playback frame rate is 5 frames/s.

456 **Video S2. The sperm pronucleus remains small leading to centrosome detachment in hybrids of *C. brenneri***
457 **females and *C. elegans* males (related to Figure 2C-E and Figure S2B,B')**. Representative timelapse sequences
458 showing centriole position and nuclear size during the first cell division in a *C. elegans* embryo (*top row*) and a *C.*
459 *brenneri* x *C. elegans* hybrid (*bottom row*). Still images of the wild-type and hybrid embryos shown are also included
460 in *Figure 1D,E* and *Figure S2B,B'*. Yellow arrows point to the centrosomes. Black dotted lines trace the outline of
461 the pronuclei. Movies are composed of a single z DIC slice overlaid with fluorescence maximum intensity projections
462 of 19 x 1.5 um z-stacks acquired every 30 seconds. Playback rate is 5 frames/s.

463

464 **Video S3. Aberrant spindle morphologies are observed in s of *C. brenneri* females and *C. elegans* males**
465 **(related to Figure 3C,D and Figure S2D).** Representative timelapse sequences showing centrioles (*green*) and
466 microtubules (*red*) in reference *C. brenneri* (first column) and *C. elegans* (second column) embryos along with two
467 *C. brenneri* x *C. elegans* hybrids. Sequences run from ooctye pronuclear appearance through the first cell division.
468 Still images of the embryos shown are also included in *Figure 3D*. The centrioles (*yellow arrows*), aberrant spindle
469 morphology (*cyan arrows*), and meiotic spindle capture (*dark blue arrows*) are indicated. A 27 x 1 µm z-stack was
470 collected every minute, and movies are composed of maximum intensity projections of the subset of z-planes that
471 best show centrosomes and spindles for each timepoint. Intensity values for spindles are not comparable between
472 different embryos because of the variable amount of dye that may enter the embryo. Playback speed is 5 frames/s.

473

474 **Video S4. A similar suite of early defects is observed in hybrids between *C. brenneri* females and males**
475 **from three Elegans group species (related to Figure 4C,D, Figure 1D,F, Figure S1C,E and Figure S3A).**
476 Representative timelapse sequences of the early embryonic cell divisions in wild-type *C. brenneri*, *C. sp. 48*, *C.*
477 *remanei* and *C. elegans* embryos (top row) along with their hybrids (*bottom row*). Still images of embryos shown
478 are also included in *Figure 4C*, *Figure S1C* (*Disorganized/other)* and *Figure S3A*. Black dotted lines trace pronuclei.
479 Movies are composed of single z slices chosen from 26 x 1 µm z-stacks acquired every 30sec. Playback rate is 5
480 frames/s.

481

482 **Table S1.** Description of manual scoring data and measured features to Figures 3 and 4 and STAR
483 Methods. In the All Scored Embryos tab, each cross type is highlighted in a different color. In the
484 Considered Phenotypes tab, rows highlighted in yellow consistently showed a phenotype during embryo
485 scoring.

486

STAR METHODS

RESOURCE AVAILABILITY

Lead contact

Further information and requests for resources and reagents should be directed to and will be fulfilled by the lead contact, Scott Rifkin ([31,32]).

Materials availability

All strains and other reagents generated in this study are freely available from the lead contact upon request. *C. brenneri, C. remanei,* and *C. elegans* (*fog-2*) strains can be obtained from the Caenorhabditis Genetics Center (CGC). *C. sp. 48* was a gift from M.A. Felix.

Data and Code Availability

- The custom computer code generated for this project is publicly available through https://gitlab.com/evodevosysgroup/Bloom_etal_2024 and will be deposited at Zenodo
- Any additional information required to reanalyze the data reported in this paper will be available from the lead contact upon request

EXPERIMENTAL MODEL AND STUDY PARTICIPANT DETAILS

C. elegans strains were maintained at 20°C on standard Nematode Growth Media (NGM) plates seeded with OP50 bacteria. The genotypes of the *C. elegans* strains used in this study are described in Reagents and Resources.

METHOD DETAILS

Strains

C. brenneri was always LKC28; *C. sp. 48* was always BRC20359; *C. remanei* was always EM464, and *C. elegans* females were always JK574, which has a *fog-2* mutation that makes hermaphrodites females.

Mating

For all crosses, L4-stage females were placed with males on a 35mm plate seeded with OP50 and left overnight at 20C for mating; females were dissected the following day. A 1:2 ratio of females to males was used for all crosses except for interspecies crosses with *C. elegans* males, for which a 1:3 ratio was used because C*. elegans* males are worse at mating than dioecious males.[56,57]

Dissections

Gravid females were dissected in Boyd Buffer (59.9 mM $NaCl_2$, 32.2 mM KCl, 2.8 mM Na_2HPO4, 1.8 mM $CaCl_2$, 5mM HEPES pH 7.2, 0.2% glucose, 2.1 mM $MgCl_2$;)[42,58] and were transferred by mouth pipette to a 2% agarose pad made in Boyd Buffer for imaging. An 18x18mm coverslip was placed over the pad and the edges of the coverslip were sealed with VALAP (1:1:1 Vaseline, Lanolin, and Parafin) to prevent drying out. We compared five different osmotic support buffers (meiosis media, Boyd buffer, 0.5X Egg Salts, 0.7X Egg Salts, and 1X Egg Salts) but no rescue of early arrest phenotypes was observed for any of them.

Brood size & embryonic viability measurements

To measure the number of embryos laid and assess their viability (defined hatching), individual L4 females were placed on a 35 mm NGM plate seeded with OP50 along with 2 or 3 males (see Mating section) and left to mate overnight at 20°C. After 24 hours, the males were removed and the females were moved to a second 35mm plate. Females were transferred again to a third 35 mm plate 20 hours later (44 hours after the start of mating). After 64 hours, the females were removed from the third plate. After each transfer, the number of freshly laid embryos on the plate from which the female was removed was counted and the plate was returned to 20°C. Since viable embryos hatch within 20 hours of being laid we waited 20-24 hours after first count was made and then counted the number of hatched and unhatched embryos to measure viability.

RNA production

The *C. brenneri* orthologs of the *C. elegans par-2* and *par-6* genes were identified based on annotation in WormBase; ortholog identity was confirmed using reciprocal BLAST. DNA templates for generating dsRNAs were generated by PCR using primers designed using Primer3 (https://primer3.ut.ee/) to amplify a 400-800 bp region of each gene from genomic DNA (see KEY RESOURES Table for sequences). Primers contained T3 or T7 promoters to enable transcription reactions. Primers for dsRNAs targeting the *C. elegans* genes were the same as those employed in a prior RNAi-based screen.[48] PCR reactions were cleaned and used as templates in T3 and T7 transcription reactions. T3 and T7 RNA products were mixed at equimolar amounts, cleaned, and annealed by adding 3X Soaking buffer (32.7 mM Na_2HPO_4, 16.5 mM KH_2PO_4, 6.3 mM NaCl, 14.1 mM NH_4Cl) to a final concentration of 1X and incubating reactions at 68C for 10 minutes then 37°C for 30 minutes.

RNA interference

For *C. elegans*, larval (L4 stage) female (JK574) worms were injected with dsRNA in the body cavity and left to recover at 20°C for 4 hours before singling and mating with male *C. elegans* (JK574) worms at 20°C overnight before imaging. For *C. brenneri*, larval (L4 stage) females (LKC28) were mated to male *C. brenneri* (LKC28) worms on a 35mm OP50 plate overnight at 20°C. Gravid females were injected with

562 dsRNA in both gonad arms, left to recover for 3 hours (20°C), before singling and leaving overnight at
563 20°C for 22 hours before imaging.

564

565 **Imaging and analysis of early and late embryogenesis**

566 After mating, dissection, and mounting as described above, we monitored early embryogenesis using
567 differential interference contrast (DIC) optics to acquire 26 x 1µm z-stacks at 30-45 second intervals. In
568 most experiments, embryos were imaged through the four-cell stage. Images were acquired using either
569 an inverted Zeiss Axio Observer Z1 system equipped with a Yokogawa CSU-X1 spinning-disk, 63X 1.40
570 NA Plan Apochromat lens (Zeiss), and a QuantEm: 512SC camera (Teledyne Photometrics), or on a
571 Nikon Ti2 microscope equipped with a Yokogawa CSU-X1 spinning disk, a 60X, 1.4 NA PlanApochromat
572 lens, and an iXon Life EMCCD camera. For monitoring fluorescent marker turn-on, embryos that had
573 been filmed by DIC during early embryogenesis were allowed to develop for 20 additional hours at 20°C
574 before the acquisition of 26 x 1µm z-stack using confocal fluorescence microscopy (488 and 561 nm
575 lasers) and DIC optics. For all measurements, embryos were cropped from time-lapse series and
576 measurements were made using FIJI.[59] Table S1 has descriptions of the features scored or measured.

577

578 **Centriole Positioning in Early Hybrid Embryos**

579 *C. elegans* (OD3701) or *C. brenneri* (LKC28) males were crossed to *C. brenneri* (LKC28) or *C. elegans*
580 (JK574) females and left to mate overnight at 20°C for 24 hours. Female worms were dissected and
581 embryos mounted as described above. Embryos were imaged by collecting 19 x 1.5 µm z-stacks every
582 30 sec, capturing DIC and fluorescence (561nm laser at 15% power, 2x2 binning, 100ms exposure)
583 through the two-cell stage. FIJI was used to crop and rotate images for scoring. Centrioles were
584 considered detached when centrioles were > 9µm apart. FIJI was used to create maximum projections
585 and to scale images for figures. The image intensities were scaled to best visualize centrosome position
586 within the early embryo.

587

588 **Spindle Angle, Pronuclear Localization and Size, and Embryo Aspect Ratio Analysis**

589 Embryos were cropped from timelapse series and measurements were made using FIJI. P0 spindle angle
590 was measured relative to the long axis of the embryo; the angle was assessed from metaphase onset
591 through the following 3.5-4.5 minutes. Images were converted to maximum intensity projections, since
592 centrioles were in different z-planes for part of the first cell division, and then each embryo was scored
593 for centrosome detachment before pronuclear meeting or centrosome mis-localization at pronuclear
594 meeting. Sperm pronucleus length and width was measured at the appearance of the oocyte-derived
595 pronucleus, and sperm-derived pronuclear area was then calculated by using the equation for the area
596 of an ellipse : $\pi \frac{length}{2} \frac{width}{2}$. Embryo aspect ratio was calculated as the ratio of cross-sectional width to
597 cross-sectional length of P0 embryos.

598

599 **Centriole Positioning and Microtubule tracking**

600 *C. brenneri* (LKC28) females were crossed with *C. brenneri* (LKC28) males or *C. elegans* (OD3701)
601 males, and *C. elegans* (JK574) females were crossed with *C. elegans* (OD3701) males. Female worms
602 were dissected into 250 nM SiR-Tubulin dye (Cytoskeleton, cat# CY-SC002). To generate an agar pad
603 containing SiR-Tubulin, 15µL of 5µM dye was added on top of a 2% agarose pad made in Boyd Buffer.
604 One-cell embryos were transferred by mouth pipette, covered with an 22x22mm coverslip, and sealed

605 with VALAP before imaging. Embryos were imaged on a Nikon Ti2 microscope equipped with a
606 Yokogawa CSU-X1 (Nikon) spinning disk, a 60X, 1.4 NA PlanApochromat lens, and an iXon Life EMCCD
607 camera. A 27 x 1 µm z-stack was collected every min, capturing DIC and fluorescence (561nm at 15%
608 power, 2x2 binning, 100ms exposure, and 640nm at 40% power and 200ms exposure) through the two-
609 cell stage. Images were cropped and rotated for analysis using FIJI. Timelapse SiR-Tubulin sequences
610 were created by generating maximum intensity projections of the subset of the best subset of 14 z-slices
611 containing the spindle and were scaled to show the best signal unobscured by the SiR-Tubulin coating
612 the eggshell. Image intensities were scaled for each embryo because dye uptake could vary between
613 embryos. Centriole channel images were created using maximum projections to best capture the
614 centrioles.

615

616 **Developmental Imaging**

617 For the arrest point experiment in Fig. S1B, *C. elegans* males (OD 1719)[29] or *C. brenneri* males (LKC28)
618 were mated with *C. elegans* females (JK574) or *C. brenneri* females (LKC28) for 24hrs at 20°C. OD1719
619 animals express germ-layer markers: ectoderm (Pdlg-1::mCherry::his-72 and Pcnd-1::mCherry::his-
620 72), endoderm (Ppha-4::pha-4::GFP), and mesoderm (Phlh-1::his-72::mCherry and Phlh-1::his-72::GFP).
621 For this experiment, embryogenesis was captured by dissecting females in Boyd Buffer and transferring
622 the embryos to a 384-well imaging plate containing 70uL Boyd Buffer. Embryos were imaged over a 10-
623 hour time-course as previously described.[29]

624

625 **Immunofluorescence of Early Embryos**

626 Slides for immunofluorescence were generated by dipping in subbing solution prepared by dissolving
627 0.1g gelatin in 25 mL of distilled water heated to 60°C, cooling to 40°C, adding 0.01g chromalum, and
628 15mg poly-lysine HBr. Subbing solution was left to stir at 40°C for 2 hours before sterile filtering and
629 storage at 4°C. Slides were dipped in subbing solution heated to 50°C and allowed to dry for 6 hours. 20-
630 30 mated female animals were placed in a 4µl drop of distilled water placed in the center of the slide and
631 an 18x18 coverslip was placed on top. Worms were compressed by pushing on the coverslip with a pipet
632 tip, embryos were pushed out of the mothers, and slides were plunged into liquid nitrogen. Slides were
633 retrieved and a razor blade was used to pop the coverslips off each slide. Slides were immediately
634 immersed in -20°C cold methanol for a 15-minute fixation. Samples were fixed and stained as previously
635 described.[60] For detection of PAR-2, slides were incubated in unconjugated primary antibody (Mouse-
636 anti-PAR-2 1:1000 dilution) overnight at 4°C, washed, and then incubated with fluorescent secondary
637 antibody (Donkey-anti-Mouse-Cy5) for 30min at room temperature. To stain for centrosomes and
638 microtubules, embryos were incubated with directly-labeled α-tubulin antibodies (DM1-α-FITC 1:1000
639 dilution; Sigma Aldrich F2168) and anti-γ-tubulin-CY3 (C-terminal antigen: LDEYKAVVQKDYLTRGL;
640 1:300 dilution)[44] for 60 minutes at room temperature. Slides were washed with PBST buffer, and 1 µg/ml
641 Hoechst was added during the last 10-minute wash. Two final washes were performed and 15 µl of
642 ProLong Glass Antifade Mount (ThermoFisher) mounting and curing solution was added before covering
643 the embryos with an 18 x 18mm coverslip. The slides were left to cure at room temperature for 24 hours
644 in a dark chamber. Samples were imaged on a DeltaVision (GE Healthcare) epifluorescence scope
645 equipped with a 100X 1.4NA oil immersion objective. Images were deconvolved using SoftWoRx
646 software (Cytvia). Maximum projections were made using FIJI and image intensities adjusted for
647 visualization of signal.

648

649 **Evolutionary analysis of hybrid embryos**

650 *C. brenneri* females were mated to males of *C. sp. 48* and*C. remanei* in a ratio of 1:2 and to males of *C*
651 *elegans* in a ratio of 1:3 on individual mating plates. Plates were left overnight at 20°C for mating as
652 described above. Twenty-four hours later, embryos were dissected from gravid female animals in Boyd
653 buffer and mounted as described above. DIC images of early embryogenesis were acquired as described
654 above collecting images every 30s until the 4-cell stage or later. Embryos were cropped and rotated for
655 further analysis. Image names were anonymized by JB, and embryos scored by RG as either a 1 (display
656 phenotype) or 0 (do not display phenotype) for the phenotypes listed in Table S1.

657

658 **Divergence time estimates**

659 We downloaded complete *Caenorhabditis* genomes from https://caenorhabditis.org, extracted the
660 longest isoforms for each protein, and used Orthofinder to estimate a species tree. Branch lengths of the
661 estimated species tree represent molecular phylogenetic distance along the branch.[61] We used these
662 branch lengths to determine the relative divergence of protein coding sequences between *C. brenneri*
663 and the three other species.

664

665 **Quantification and Statistical Analysis**

666 All graphs shown in the manuscript were created and analyzed in R (Rstudio).[62]

667

668 **REFERENCES:**
669

670 1. Coyne, J. A. & Orr, H. A. Patterns of reproductive isolation in Drosophila. *Evolution* **43**, 362–381
671 (1989).
672 2. Dobzhansky, T. *Genetics and the Origin of Species, By Theodosius Dobzhansky*. (1937).
673 3. Mayr, E. *Animal Species and Evolution*. (Harvard University Press, 1963).
674 4. Sawamura, K., Taira, T. & Watanabe, T. K. Hybrid lethal systems in the Drosophila melanogaster
675 species complex. I. The maternal hybrid rescue (mhr) gene of Drosophila simulans. *Genetics* **133**,
676 299–305 (1993).
677 5. Sawamura, K., Yamamoto, M. T. & Watanabe, T. K. Hybrid lethal systems in the Drosophila
678 melanogaster species complex. II. The Zygotic hybrid rescue (Zhr) gene of D. melanogaster.
679 *Genetics* **133**, 307–313 (1993).
680 6. Forejt, J. Hybrid sterility in the mouse. *Trends in Genetics* **12**, 412–417 (1996).
681 7. Mihola, O., Trachtulec, Z., Vlcek, C., Schimenti, J. C. & Forejt, J. A Mouse Speciation Gene
682 Encodes a Meiotic Histone H3 methyltransferase. *Science* **323**, 373–5 (2009).
683 8. Barbash, D. A., Siino, D. F., Tarone, A. M. & Roote, J. A rapidly evolving MYB-related protein
684 causes species isolation in Drosophila. *Proceedings of the National Academy of Sciences of the*
685 *United States of America* **100**, 5302–5307 (2003).
686 9. Barbash, D. A., Awadalla, P. & Tarone, A. M. Functional divergence caused by ancient positive
687 selection of a Drosophila hybrid incompatibility locus. *PLoS Biology* **2**, 839–848 (2004).
688 10. Sawamura, K. & Yamamoto, M.-T. Characterization of a reproductive isolation gene, zygotic hybrid
689 rescue, of Drosophila melanogaster by using minichromosomes. *Heredity* **79**, 97–103 (1997).
690 11. Barbash, D. A. Ninety years of Drosophila melanogaster hybrids. *Genetics* **186**, 1–8 (2010).
691 12. Wittkopp, P. J., Haerum, B. K. & Clark, A. G. Evolutionary changes in cis and trans gene regulation.
692 *Nature* **430**, 85–88 (2004).
693 13. Coolon, J. D., McManus, C. J., Stevenson, K. R., Graveley, B. R. & Wittkopp, P. J. Tempo and
694 mode of regulatory evolution in Drosophila. *Genome Research* **24**, 797–808 (2014).

695 14. Bundus, J. D., Wang, D. & Cutter, A. D. Genetic basis to hybrid inviability is more complex than
696 hybrid male sterility in Caenorhabditis nematodes. *Heredity* **121**, 169–182 (2018).
697 15. Bundus, J. D., Alaei, R. & Cutter, A. D. Gametic selection, developmental trajectories, and extrinsic
698 heterogeneity in Haldane's rule. *Evolution* **69**, 2005–2017 (2015).
699 16. Dey, A., Jin, Q., Chen, Y. C. & Cutter, A. D. Gonad morphogenesis defects drive hybrid male
700 sterility in asymmetric hybrid breakdown of Caenorhabditis nematodes. *Evolution and Development*
701 **16**, 362–372 (2014).
702 17. Bi, Y. *et al.* A Genome-Wide Hybrid Incompatibility Landscape between Caenorhabditis briggsae
703 and C. nigoni. *PLoS Genetics* **11**, 1–26 (2015).
704 18. Baugh, L. R., Hill, A. A., Slonim, D. K., Brown, E. L. & Hunter, C. P. Composition and dynamics of
705 the *Caenorhabditis elegans* early embryonic transcriptome. *Development* **130**, 889–900 (2003).
706 19. Guven-Ozkan, T., Nishi, Y., Robertson, S. M. & Lin, R. Global Transcriptional Repression in C.
707 elegans Germline Precursors by Regulated Sequestration of TAF-4. *Cell* **135**, 149–160 (2008).
708 20. Stoeckius, M., Grün, D. & Rajewsky, N. Paternal RNA contributions in the Caenorhabditis elegans
709 zygote. *The EMBO Journal* **33**, 1740–1750 (2014).
710 21. Macchietto, M. *et al.* Comparative Transcriptomics of Steinernema and Caenorhabditis Single
711 Embryos Reveals Orthologous Gene Expression Convergence during Late Embryogenesis.
712 *Genome Biology and Evolution* **9**, 2681–2696 (2017).
713 22. Cowan, C. R. & Hyman, A. A. Centrosomes direct cell polarity independently of microtubule
714 assembly in C. elegans embryos. *Nature* **431**, 92–96 (2004).
715 23. Rose, L. & Gonczy, P. Polarity establishment, asymmetric division and segregation of fate
716 determinants in early C. elegans embryos. *WormBook* 1–43 (2014) doi:10.1895/wormbook.1.30.2.
717 24. Baird, S. E. & Yen, W. C. Reproductive isolation in Caenorhabditis: Terminal phenotypes of hybrid
718 embryos. *Evolution and Development* (2000) doi:10.1046/j.1525-142X.2000.00031.x.
719 25. Baird, S. E. & Seibert, S. R. Reproductive isolation in the Elegans-Group of Caenorhabditis. **5**, 18–
720 25 (2013).

721 26. Rockman, M. V. *et al.* A phylogeny and molecular barcodes for Caenorhabditis, with numerous new
722 species from rotting fruits. *BMC Evolutionary Biology* **11**, 339 (2011).
723 27. Cutter, A. D., Garrett, R. H., Mark, S., Wang, W. & Sun, L. Molecular evolution across
724 developmental time reveals rapid divergence in early embryogenesis. 359–373 (2019)
725 doi:10.1002/evl3.122.
726 28. Landry, C. R. *et al.* Compensatory cis-trans Evolution and the Dysregulation of Gene Expression in
727 Interspecific Hybrids of Drosophila. **1822**, 1813–1822 (2005).
728 29. Wang, S. *et al.* A high-content imaging approach to profile *C. elegans* embryonic development.
729 *Development* dev.174029 (2019) doi:10.1242/dev.174029.
730 30. Green, R. A. *et al.* Automated profiling of gene function during embryonic development. *Cell* **187**,
731 3141-3160.e23 (2024).
732 31. Memar, N. *et al.* Twenty million years of evolution: The embryogenesis of four Caenorhabditis
733 species are indistinguishable despite extensive genome divergence. *Developmental Biology* 1–18
734 (2018) doi:10.1016/j.ydbio.2018.12.022.
735 32. Levin, M., Hashimshony, T., Wagner, F. & Yanai, I. Developmental Milestones Punctuate Gene
736 Expression in the Caenorhabditis Embryo. *Developmental Cell* **22**, 1101–1108 (2012).
737 33. Boveri, T. Zellenstudien II: Die Befruchtung und Teilung des Eies von Ascaris megalocephala.
738 *Jenaer Zeitschrift für Naturwissenschaft* 685–882, plates XIX-XXIII (1888).
739 34. Albertson, D. G. Formation of the first cleavage spindle in nematode embryos. *Developmental*
740 *Biology* **101**, 61–72 (1984).
741 35. Oegema, K. Cell division. *WormBook* (2006) doi:10.1895/wormbook.1.72.1.
742 36. McNally, K. L. P. *et al.* Kinesin-1 Prevents Capture of the Oocyte Meiotic Spindle by the Sperm
743 Aster. *Developmental Cell* **22**, 788–798 (2012).
744 37. Severson, A. F., Von Dassow, G. & Bowerman, B. Oocyte Meiotic Spindle Assembly and Function.
745 in *Current Topics in Developmental Biology* vol. 116 65–98 (Elsevier, 2016).

746 38. Cuenca, A. A., Schetter, A., Aceto, D., Kemphues, K. & Seydoux, G. Polarization of the C. elegans
747 zygote proceeds via distinct establishment and maintenance phases. *Development* **130**, 1255–
748 1265 (2003).
749 39. Munro, E., Nance, J. & Priess, J. R. Cortical Flows Powered by Asymmetrical Contraction Transport
750 PAR Proteins to Establish and Maintain Anterior-Posterior Polarity in the Early C. elegans Embryo.
751 *Developmental Cell* **7**, 413–424 (2004).
752 40. Bienkowska, D. & Cowan, C. R. Centrosomes Can Initiate a Polarity Axis from Any Position within
753 One-Cell C. elegans Embryos. *Current Biology* **22**, 583–589 (2012).
754 41. Hoege, C. & Hyman, A. A. Principles of PAR polarity in Caenorhabditis elegans embryos. *Nat Rev*
755 *Mol Cell Biol* **14**, 315–322 (2013).
756 42. Boyd, L., Guo, S., Levitan, D., Stinchcomb, D. T. & Kemphues, K. J. PAR-2 is asymmetrically
757 distributed and promotes association of P granules and PAR-1 with the cortex in *C. elegans*
758 embryos. *Development* **122**, 3075–3084 (1996).
759 43. Hoege, C. *et al.* LGL Can Partition the Cortex of One-Cell Caenorhabditis elegans Embryos into
760 Two Domains. *Current Biology* **20**, 1296–1303 (2010).
761 44. Hannak, E., Kirkham, M., Hyman, A. A. & Oegema, K. Aurora-A kinase is required for centrosome
762 maturation in *Caenorhabditis elegans*. *The Journal of Cell Biology* **155**, 1109–1116 (2001).
763 45. Hamill, D. R., Severson, A. F., Carter, J. C. & Bowerman, B. Centrosome Maturation and Mitotic
764 Spindle Assembly in C. elegans Require SPD-5, a Protein with Multiple Coiled-Coil Domains.
765 *Developmental Cell* **3**, 673–684 (2002).
766 46. Hannak, E. *et al.* The kinetically dominant assembly pathway for centrosomal asters in
767 *Caenorhabditis elegans* is γ-tubulin dependent. *The Journal of Cell Biology* **157**, 591–602 (2002).
768 47. Ohta, M. *et al.* Polo-like kinase 1 independently controls microtubule-nucleating capacity and size of
769 the centrosome. *Journal of Cell Biology* **220**, e202009083 (2021).
770 48. Sönnichsen, B. *et al.* Full-genome RNAi profiling of early embryogenesis in Caenorhabditis
771 elegans. *Nature* **434**, 462–469 (2005).

772 49. Grill, S. W., Gönczy, P., Stelzer, E. H. K. & Hyman, A. A. Polarity controls forces governing
773 asymmetric spindle positioning in the Caenorhabditis elegans embryo. *Nature* **409**, 630–633
774 (2001).
775 50. Malone, C. J. *et al.* The C. elegans Hook Protein, ZYG-12, Mediates the Essential Attachment
776 between the Centrosome and Nucleus. *Cell* **115**, 825–836 (2003).
777 51. Minn, I., Rolls, M. M., Hanna-Rose, W. & Malone, C. J. SUN-1 and ZYG-12, Mediators of
778 Centrosome–Nucleus Attachment, Are a Functional SUN/KASH Pair in Caenorhabditis elegans.
779 *MBoC* **20**, 4586–4595 (2009).
780 52. Gönczy, P., Pichler, S., Kirkham, M. & Hyman, A. A. Cytoplasmic Dynein Is Required for Distinct
781 Aspects of Mtoc Positioning, Including Centrosome Separation, in the One Cell Stage
782 *Caenorhabditis elegans* Embryo. *The Journal of Cell Biology* **147**, 135–150 (1999).
783 53. Meyerzon, M. *et al.* Centrosome attachment to the C. elegans male pronucleus is dependent on the
784 surface area of the nuclear envelope. *Developmental Biology* **327**, 433–446 (2009).
785 54. Cheng, N. N., Kirby, C. M. & Kemphues, K. J. Control of Cleavage Spindle Orientation in
786 Caenorhabditis elegans: The Role of the Genes par-2 and par-3.
787 55. McNally, K. L. & McNally, F. J. Fertilization initiates the transition from anaphase I to metaphase II
788 during female meiosis in C. elegans. *Developmental Biology* **282**, 218–230 (2005).
789 56. Anderson, J. L., Morran, L. T. & Phillips, P. C. Outcrossing and the Maintenance of Males within C.
790 elegans Populations. *Journal of Heredity* **101**, S62–S74 (2010).
791 57. Ebert, M. S. Evolution remodels olfactory and mating-receptive behaviors in the transition from
792 female to hermaphrodite reproduction. *OPEN ACCESS*.
793 58. Bao, Z. & Murray, J. I. Mounting *Caenorhabditis elegans* Embryos for Live Imaging of
794 Embryogenesis: Figure 1. *Cold Spring Harb Protoc* **2011**, pdb.prot065599 (2011).
795 59. Schindelin, J. *et al.* Fiji: an open-source platform for biological-image analysis. *Nat Methods* **9**, 676–
796 682 (2012).

797 60. Oegema, K., Desai, A., Rybina, S., Kirkham, M. & Hyman, A. A. Functional Analysis of Kinetochore
798 Assembly in *Caenorhabditis elegans*. *The Journal of Cell Biology* **153**, 1209–1226 (2001).
799 61. Emms, D. M. & Kelly, S. OrthoFinder: phylogenetic orthology inference for comparative genomics.
800 *Genome Biol* **20**, 238 (2019).
801 62. R Core Team. R: A Language and Environment for Statistical Computing. R Foundation for
802 Statistical Computing (2023).
803